Since January 2020 Elsevier has created a COVID-19 resource centre with free information in English and Mandarin on the novel coronavirus COVID-19. The COVID-19 resource centre is hosted on Elsevier Connect, the company's public news and information website.

Ultramicroscopy 135 (2013) 99–104

Contents lists available at ScienceDirect

Ultramicroscopy

journal homepage: www.elsevier.com/locate/ultramic

Short communication

Nanofabrication of a gold fiducial array on specimen support for electron tomography

Roman I. Koning [a,*], Vladimir G. Kutchoukov [b], Cornelis W. Hagen [b], Abraham J. Koster [a]

[a] Leiden University Medical Center, Department of Molecular Cell Biology, Section Electron Microscopy, P.O. Box 9600, 2300 RC Leiden, The Netherlands
[b] Delft University of Technology, Faculty of Applied Sciences, Charged Particle Optics, Lorentzweg 1, 2628 CJ Delft, The Netherlands

ARTICLE INFO

Article history:
Received 24 April 2013
Received in revised form
19 June 2013
Accepted 25 June 2013
Available online 16 July 2013

Keywords:
Lithography
MEMS
Cryo-electron microscopy
Electron tomography
patterning
Gold fiducials
TEM

ABSTRACT

Here we describe the production, using lithography and micro-engineering technologies, of patterned arrays of nanofabricated gold dots on a thin Si_3N_4 electron transparent layer, supported by silicon. We illustrate that the support with a patterned structure of nanosized gold can be exploited for (cryo) electron tomography application as a specimen support with predefined alignment markers. This nanogold patterned support has several advantages. The Si_3N_4 window provides a 50 nm thin, strong and flat support with a ~0.7 mm^2 large electron-beam transparent window. The nanogold pattern has a user-defined size and density, is highly regular and stable. This facilitates accurate tracking during tilt series acquisition, provides sufficient contrast for accurate alignment during the image reconstruction step and avoids an uneven lateral distribution and movement of individual fiducials. We showed that the support is suitable for electron tomography on plastic sections.

1. Introduction

Electron tomography is a technique for three-dimensional visualization of cellular structures and macromolecular arrangements at nanometer resolution. With electron tomography, the architecture of plastic embedded and stained sections of cells, as well as the molecular structural arrangements within thin areas of vitrified cells and cryo-sections of high-pressure frozen cells and tissues, can be investigated in three dimensions. During the last decade, for a wide variety of biological systems the ultrastructure of cells, cellular organelles and their molecular components have been successfully investigated and have given great insights into cellular structure and function [1,2].

One of the parameters that define the quality of tomograms acquired with transmission electron microscopy (TEM) is the accuracy by which the individual images of an acquired tilt series can be aligned relative to each other. This alignment step can be performed in several ways. One approach is to make use of cross-correlation between pairs of individual images in the acquired tilt series. Here, the relative shifts between the images are computed making use of the inherent image contrast generated by the electron microscope specimen. This approach is often referred to as fiducial-less alignment. Another, more often used, approach makes use of fiducial markers that are deposited on the specimen support. In this approach the locations of the markers are used for alignment of the tilt series. In most cases, these fiducial markers are nanometer sized (ranging from 5 to 20 nm) spherical gold beads [3] that provide high contrast. Suspensions of (protein-stabilized) gold beads are added to and mixed with the sample or applied onto the specimen support film prior to adding the sample. An advantage of this fiducial-marker approach is that it allows retrieving not only image shifts, but that it is also a suitable approach to determine image rotations and local image distortions based on a geometrical model of the specimen tilting. Disadvantage of the fiducial marker approach is that the spatial distribution and amount of gold beads on the specimen support is hard to control. The unpredictable amount of markers and irregular distribution can result in areas on the specimen support that are suboptimal for tracking during data collection and for alignment during image reconstruction. Additionally, it is known that individual gold fiducials can move during data acquisition, both on cryo-sections which can suffer random distortions [4] and on plastic sections due to shrinkage [5,6]. This leads to an imperfect alignment of the acquired tilt series. Therefore, control over the size, concentration and positioning of fiducials on the support, as well as the firm attachment to the support would be advantageous for accurate tracking and alignment in electron tomography. Different nanofabrication techniques have been applied to engineer nano-patterns [7] and even nanogold arrays [8] on silicon surfaces, for applications in cell biology and electronics and optics [9].

We present an electron beam lithography technique to produce patterned nanogold surfaces. This enabled full control to make specific patterns of gold (30–50 nm) with a relatively wide spacing

* Corresponding author. Tel.: +31 71 526 9296; fax: +31 71 526 8271.
E-mail addresses: r.i.koning@lumc.nl, r.i.koning@gmail.com (R.I. Koning).

0304-3991/$ - see front matter © 2013 Elsevier B.V. All rights reserved.
http://dx.doi.org/10.1016/j.ultramic.2013.06.015

(0.2–5.0 μm) on a 50 nm thin electron transparent silicon nitride membrane of 417 × 817 μm that is supported by silicon, as required for use as fiducials in electron tomography. These silicon-based supports have the advantages that they are flat and strong, that the electron beam transparent window is not obstructed by grid bars and that the size and positioning of fiducial markers is predefined. The advantages of the patterned gold are that fiducials are evenly spread in a predefined pattern and density, and that they are firmly attached to the highly flat support, avoiding possible movement of individual fiducials. We show that the patterned gold dots can be used as fiducials to facilitate sample tracking during tomographic tilt series acquisition and for accurate alignment during tomographic reconstruction.

2. Materials and methods

2.1. The production of Si_3N_4 windows in silicon wafers

The silicon nitride windows are fabricated on 200 μm thick 4 inch (100)-silicon wafers (Fig. 1, top row). LPCVD (low-pressure chemical vapor deposition) silicon nitride with a thickness of 50 nm is deposited on the wafer. Since the deposition takes place in a furnace (Tempress Systems) the wafer is coated from both sides. In the next lithography step windows are opened in the photoresist layer (ZEP 520), defining the different chips and the transparent membrane locations. The pattern was written by using electron beam lithography with 100 keV beam energy. In order to reduce the writing time the pattern consisted of small squares and diagonals. However, mask contact lithography could be used in case of mass production (where a fixed design is used) to reduce the cost. After development the nitride layer was patterned by dry etching, using CHF_3/Ar chemistry. The nitride layer serves as a mask during the consequent wet etching step with KOH solution (30 wt%, 83 °C). The etch rate of silicon nitride in KOH is less than 1 nm/h and can be neglected. Etch rates for silicon, silicon nitride and silicon dioxide are varying with concentration and temperature of KOH [10,11]. The silicon etches anisotropically along the (111)-plane in KOH, with an angle of 54.7° from the (100)-plane. Once the wafer is etched through down to the silicon nitride layer on the opposite site, the etching is stopped. After cleaning and drying the wafer, patterns of gold markers are produced on the silicon nitride window. After that the different support samples are separated from the wafer by breaking along the predefined scribe lines.

2.2. The production of gold marker patterns on Si_3N_4 windows

The gold marker patterns are produced using a combination of electron beam lithography (EBPG) and metal evaporation (Fig. 1A). First, a 350 nm thick layer of polydi(m)ethyl glutarimide (PMGI, 7% in anisol) and 60 nm polymethyl-methacrylate (PMMA, 950 K, 2% in anisol) was deposited by spin-coating on a 50 nm thick Si_3N_4 membrane (Fig. 1B). To facilitate the removal of both layers by a lift-off process the PMGI layer is etched away under the PMMA layer. Both layers are subsequently prebaked – PMGI at 200 °C for 15 min and the PMMA layer had to harden by baking it at 175 °C for at least 60 min to prevent it later from collapsing after development of the PMGI layer. Then a pattern of dots of two different sizes with diameters of ~30 nm for TEM imaging and ~250 nm for light microscopy and low magnification TEM imaging are written by exposure of the Si_3N_4/PMGI/PMMA to a 100 keV electron beam. The electron beam exposure dose for the small dots was in the range of 40,000 μC/cm^2. The pattern consisted of 10 nm diameter dots with a 500 nm pitch. After electron beam etching and dry etching the exposure the irradiated PMMA is removed by solubilization in 25% methylisobutylketone (MIBK) in isopropylalcohol (IPA). In order to get a good pattern resolution a developer temperature of 5 °C and a development time of 150 s were used. In the next step the PMGI was etched under the PMMA layer using MF-321 developer (Sigma-Aldrich). The etching time was found to be very critical. Too short times resulted in a not completely developed PMGI layer and too long times resulted in the collapse

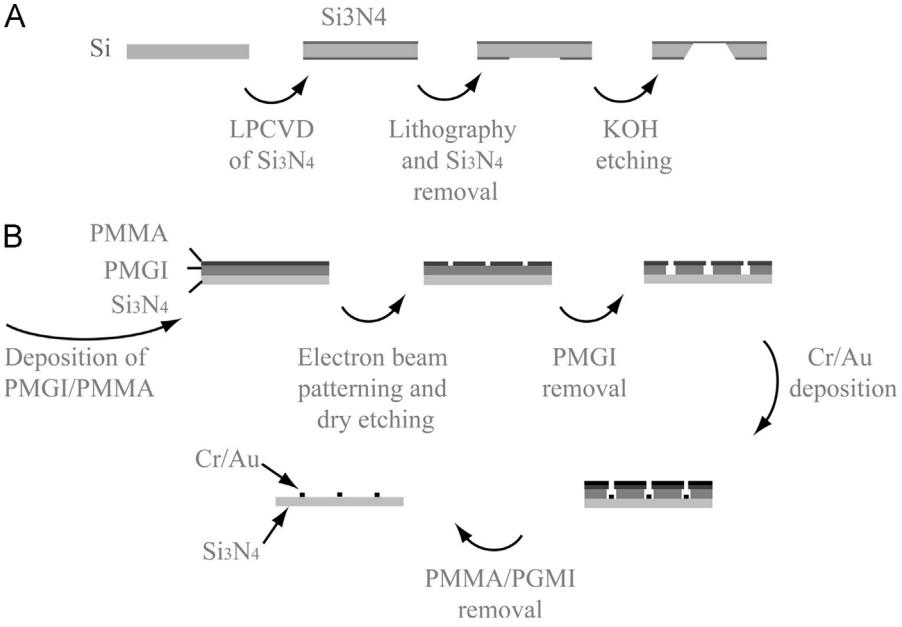

Fig. 1. Schematic fabrication of the production of gold marker patterns on silicon nitride windows on silicon wafers. (A) On a (100)-silicon wafer a 50 nm thick layer of Si_3N_4 is deposited on both sides of the wafer by low pressure chemical vapor deposition (LPCVD). A Si_3N_4 window is created by electron beam lithography and dry etching. The silicon is removed by KOH wet etching. (B) On the 50 nm silicon nitride window a 350 nm layer of PMGI and a 60 nm layer of PMMA are deposited by spin coating. A desired pattern of 10 nm spots is written by an electron beam. The exposed areas of the top PMMA layer are removed. The PMGI underlying the open areas in the PMMA layer is chemically washed away. A 5 nm layer of chrome and a 15 nm gold layer are evaporated (onto the Si_3N_4 window). The PMGI/PMMA with the Cr/Au is removed and the pattern of gold dots on the Si_3N_4 window remains.

of the PMMA. The optimal etching time was found to be 18 s. In the next step subsequently 5 nm of chromium and 15 nm of gold are deposited by evaporation (Temescal electron beam evaporator) on the sample. The chromium was needed for proper adhesion between the Si_3N_4 window and the gold. The deposition rates were kept as low as possible in order to minimize heating of the PMMA. Finally, the PMMA and PMGI are removed in 1-methyl-2-pyrrolidinone. The smallest dots that are produced in the above described manner have a diameter of about 30 nm. The bigger gold structures of ~250 nm in the pattern are written in PMMA at a dose of 18,000 $\mu C/cm^2$.

2.3. Design of the nanogold array on silicon nitride as support for electron microscopy specimens

For electron tomography applications the design of the silicon nitride support with nanofabricated arrays of gold dots had to meet several criteria. The silicon nitride on which the nanogold array is placed should be thin to be sufficiently electron transparent. Furthermore, the window should be large enough to allow tilt angles up to 60° without obstructing the view by the supporting silicon during electron tomography acquisition. Therefore, silicon nitride electron transparent windows of 50 nm thickness were made on (100) silicon wafers of 200 μm thickness. A mask of 700 × 1100 μm was written in the silicon wafer, which after KOH etching resulted in a 417 × 817 μm transparent Si_3N_4 window. The electron beam passing through the center of the Si_3N_4 windows can pass unobstructed up to 68° tilts. Several viewing windows were produced on one silicon wafer, which were separated by etched scribe lines, delineating squares of 2.15 × 2.15 mm (resulting in a diagonal size of 3.05 mm). The scribe lines facilitated separation of the silicon wafer into smaller pieces that fitted standard TEM holders.

An area of 0.25 × 0.50 mm was covered with an array of ~30 nm gold dots with a spacing of 0.50 μm (Fig. 2 B, E and F). The corners of this array were marked by large squares that were visible in a light microscope (Fig. 2A and D). The positioning of the nanogold in the array was performed with a precision of ~23 nm, as can be seen from a Fourier transform of part of the array. (Fig. 2C).

Alternatively, a support was produced with a matrix with 101 × 101 gold clusters in three different sizes: 50 nm dots with a 200 nm distance between them, 200 nm dots every 1000 nm, and 500 nm dots every 5000 nm (Fig. 2H and I).

2.4. Specimen preparation of the biological resin-embedded and stained section

The preparation of the biological sections was described earlier [12]. Briefly, Vero E6 cells were grown on Thermanox and infected with SARS-CoV at a MOI (multiplicity of infection) of 10. Next, because of safety regulations, samples were chemically pre-fixed at 7 h post-infection with 3% paraformaldehyde in PHEM-buffer. After chemical fixation, the sample was plunge-frozen in a plunge-

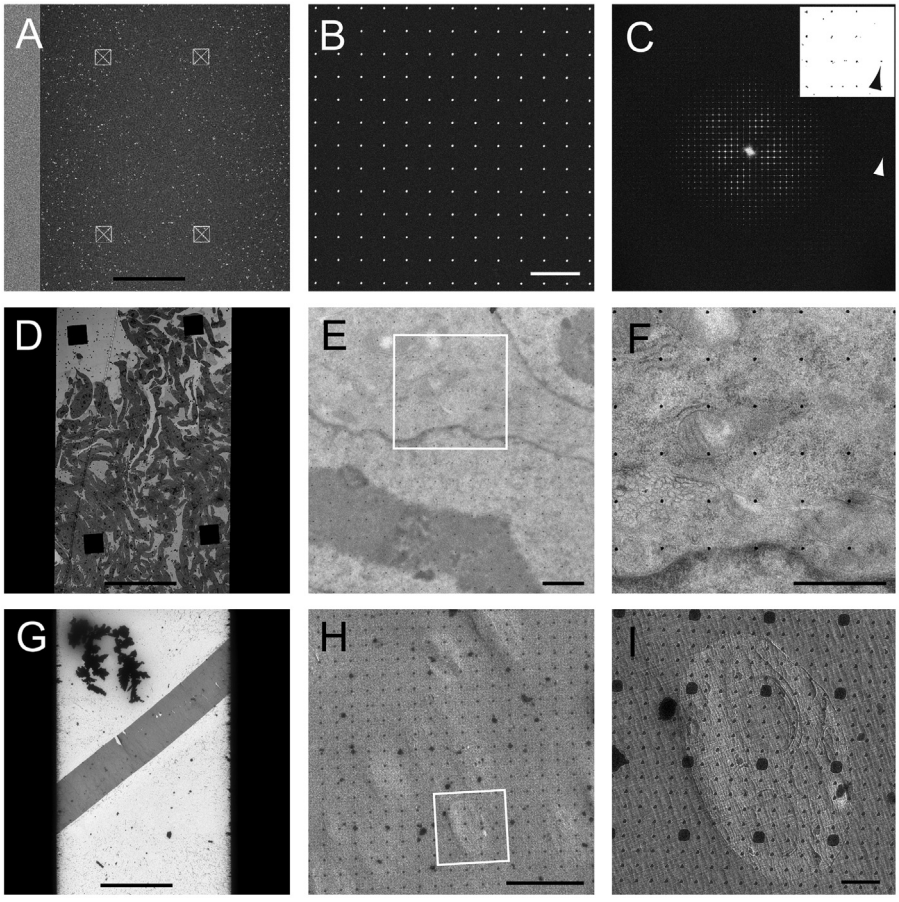

Fig. 2. Silicon nitride support with gold markers imaged in SEM: (A) at low magnification large markers are present that mark the position of the array, white dots are due to contamination. (B) shows the array at larger magnification, (C) the Fourier transform of (B) and inset (magnified and contrast inverted part from C) show that the array is ordered to the 22nd reflection at ~22 nm (arrowheads). (D) Plastic embedded and sectioned cells are positioned on the silicon nitride support (large black squares are markers for LM). (E) At higher magnification a cell nucleus is positioned on the support and in (F) (magnified from white box in E) several mitochondria can be observed. (G) Also cryo-sections can be positioned on a silicon nitride membrane. (H) A cryo-section is positioned over an array with different sizes of gold markers. (I) A cryo-sectioned malaria infected red blood cell is imaged. Scale bars are 200 μm (A, D and G), 1 μm (B, E, F), 5 μm (H) and 500 nm (I).

freezer device at 100% air humidity. Afterwards, the sample was freeze-substituted overnight with 1% osmiumtetraoxide, 0.5% uranylacetate and 10% water dissolved in acetone. Then, at room temperature, samples were infiltrated with epoxy LX-12 resin and polymerized at 60 °C. Thick sections of 200 nm were cut with a Leica UC6 ultramicrotome and dried onto the silicon nitride support.

2.5. Specimen preparation of the cryo-sectioned frozen-hydrated material

High pressure frozen (Leica Empact 2) malaria infected red blood cells were cryo-sectioned with a nominal thickness of 50 nm in a Leica EM UC6 ultramicrotome (Leica Microsystems) at −140 °C, a cutting speed of 1.0 mm/s, using a diamond knife (Diatome) in combination with a charging device (Simco). The positioning of the frozen-hydrated sections on silicon grids was facilitated by the visibility of the 250 nm sized dots on the support.

2.6. Electron tomographic data collection on the resin-embedded section

Electron tomographic data collection on the plastic embedded sections was performed on FEI Tecnai 12 BioTwin TEM with a LaB_6 filament operated at 120 kV, equipped with a 4k × 4k FEI Eagle camera, or on a Tecnai 20 TEM with a FEG operated at 200 kV equipped with a Gatan GIF 2001 with a 2k × 2k camera. Tilt series were recorded using Xplore3D software (FEI), at 1 μm under focus, every 1° from −60° to +60° at 10,000× to 30,000× magnification. The pixel size of the 4k × 4k images ranged from 0.42 to 1.31 nm. Cryo-electron microscopy was performed using a Gatan 914 high tilt cryo-holder.

2.7. Electron tomographic image reconstruction

The tomographic tilt series were processed using IMOD version 3.13 [13]. The individual images within the tilt series were preprocessed by hot pixel removal. Next, the series was aligned using the cross-correlation functionality. Final accurate alignment was performed by tracking the deposited gold dots on the Si_3N_4, as fiducial markers. Finally, during the tomographic reconstruction step, the intensity from to the fiducials was removed. The tomograms were calculated using weighted back-projection.

3. Results and discussion

3.1. Attachment of the plastic and cryo-sections on the nanopatterned support

To make use of the nanogold arrayed support for electron tomography we evaluated its use for plastic sections of fixed, resin embedded and stained cells and also for cryo-sectioned cells. High pressure frozen freeze-substituted plastic embedded 200 nm thick sectioned SARS-CoV infected Vero cell sections could be placed on the silicon nitride window with the nanogold array without any special precautions. To guide the positioning of the sections four markers were used that are visible by eye (Fig. 2D). In the transmission electron microscope the sections can be seen being placed over the nanogold array (Fig. 2E and F). The advantage is that the silicon nitride support is very flat and spans millimeter long distances without obstruction of grid bars. Hereby the field of view in the electron microscope is optimized and suitable for high specimen tilts during tomography. Consequently, the specimen area that can be used for data collection will be larger than the case for conventional carbon carriers.

Cryo-sections of high pressure frozen malaria infected red blood cells were also attached over the array. Cryo-sections were positioned on a designed support of a matrix with 101 × 101 gold clusters in three different sizes (Fig. 2G–I). Firm attachment of the cryo-section to the support is important for electron tomography data acquisition since the fiducials are present on the specimen support and have to be in close proximity to the section in order to use them for tilt series alignment. For this purpose, a charging device was used to attach these to the support [14]. However, using the charging device the cryo-sections attached readily to the silicon support, but not to the silicon nitride window. Evaporation of an additional layer of carbon on top of the silicon nitride window had the effect that the sections not only attached firmly to the silicon support, but also to the carbon coated silicon nitride window.

In our hands, silicon-based supports are difficult to handle for cryo-EM. They are relatively thick and cumbersome to mount in the currently available standard cryo-electron microscopy holders. Silicon is firm and brittle and consequently the supports break easily upon clamping into the cryo-holder. In addition, the thin silicon nitride viewing windows are still relatively thick (50 nm) compared to standard carbon support films (~10 nm). This thickness leads to increased noise levels in the cryo-electron microscopy images, resulting in a decreased resolution. Furthermore we noticed that cryo-sections attached irreproducibly to the Si_3N_4 window and charging and heating effects under the electron beam were observed. Nevertheless, these disadvantages can be solved by dedicated engineering. For example by nanopatterning on other types of available support, like TiSi metal glass [15], holey carbon or graphene.

3.2. Electron tomography using the nanogold array

The produced nanopatterned gold on Si_3N_4 windows were used as fiducials in electron tomography to enable tracking during tilt series acquisition and alignment on stained sections of biological material (Fig. 3). Image tracking during tilt series acquisition was effective between 5000× and 20,000× magnification. At higher magnification, the number of fiducials that are visible within the field of view of the image detector became too low (less than 5), especially for alignment during reconstruction. Even at very low electron dose imaging conditions (0,10 s exposure time, spot 11 and a spread beam resulting in minimal camera counts (~8 counts per pixel), the automated data acquisition tracking software performed accurately and reliably. The regular distribution of fiducials enables tomography with equal alignment quality independent of the position on sample, which is not always the case for unequally distributed gold fiducials when applied from a suspension of nanogold.

During the tomographic reconstruction step, the fine alignment of the tilt series using IMOD was performed using all fiducial markers visible in the field of view during the whole tilt series (Fig. 3C). The nanogold fiducials have the shape of flattened disks and appear as ovals at high specimen tilts. In spite of this difference compared to the spherical gold beads that are normally used as fiducial markers, the alignment software was able to determine the center of mass of the non-spherical markers and could use them for automatic tracing and alignment. Removal of gold beads was performed to remove projection artifacts during tomographic reconstruction. A virtual slice through the tomogram shows the cellular membranes, vesicles and rough endoplasmatic reticulum with ribosomes (Fig. 3D).

The localization accuracy of the fiducials (which was 22 nm) on the flat Si_3N_4 surface provides a potential means for measurement and correction of electron optical image distortions [16]. Since the positioning of the array of fiducials is controlled with nanometer precision, and the pattern is fixed to the support, it will remain

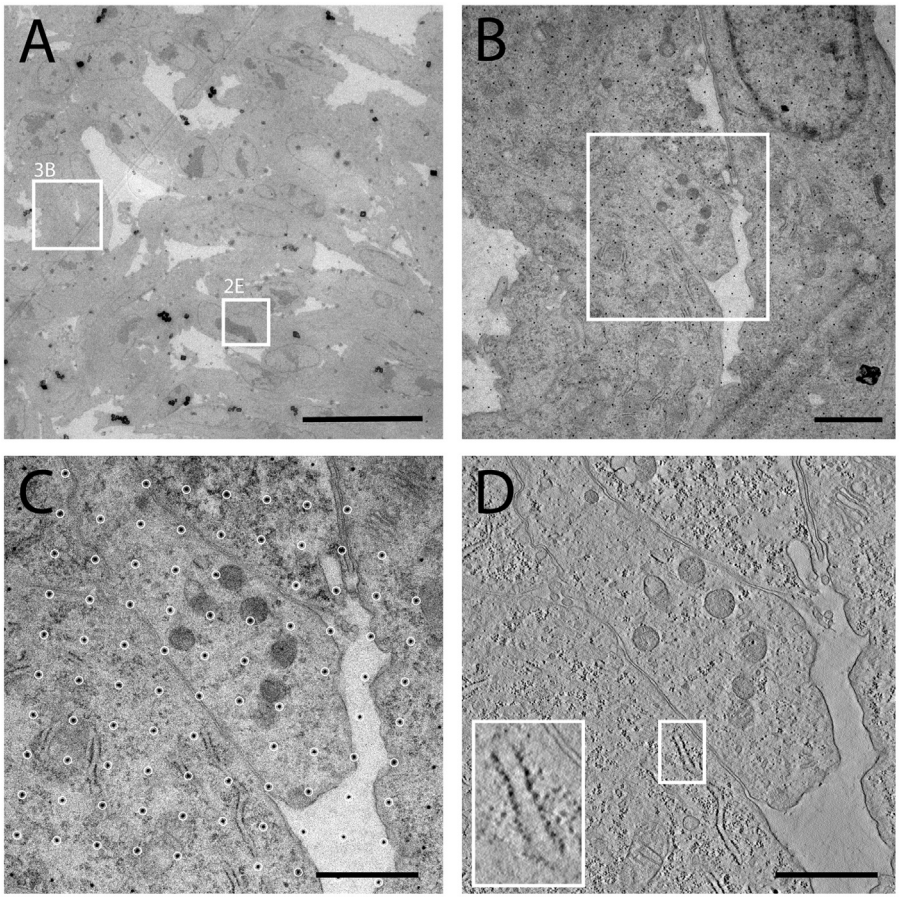

Fig. 3. Tomograms were recorded using the gold array as fiducials. (A) Overview of the area where images were recorded (small white box: Fig. 2E and large white box: (B, this figure)). (B) Area (white box) where tomogram was recorded. (C) Optimized positions (white circles) of fiducials (black dots) after fine alignment. (D) Tomographic slice from tomogram showing ribosomes on endoplasmatic reticulum (inset). Scale bars are 20 μm (A), 2 μm (B) and 1 μm (C, D).

unchanged (no shrinkage or other beam-induced effects) at all specimen tilt angles. This allows for precise rotation and magnification correction during tilt series alignment. Additionally, it enables tilt angle determination from individual images, which is currently not possible when using gold fiducials from suspension due to imaging dependent marker movement and non-flatness of the support.

We believe that method that we applied for the fabrication of the patterned nanogold can still be improved. With the specimens we used, the individual dots were produced using electron beam lithography in a Vistec EBPG, which sets a limits to the fabrication speed of the specimen support. In addition, the production of the gold patterns required some tuning of the exposure and development times to obtain sets of reproducible adequately shaped gold dots. Another current disadvantage is the relative large size of the gold dots used. While gold fiducials in electron tomography are generally between 5 and 15 nm, the minimal size of the currently used dots are about 25 nm. Recently, it was show that new NEMS techniques are available to produce smaller dots in the size range of 5–10 nm [15]. For a large scale production of these type of carriers, techniques have to be developed that enable to write large areas of dots on the viewing windows. One approach could be to use a multi-beam scanning electron microscope [17].

4. Conclusions

We explored the use of nanofabricated arrays of gold on a silicon based support for their use as fiducials in electron tomography. The main advantage of the nanofabricated patterned gold clusters on silicon based support for tomography is that the position, size and amount of fiducials can be controlled and they are rigidly attached to the support. This array of gold dots on an electron transparent silicon nitride support provided fiducial markers that can be exploited for alignment procedures during acquisition and reconstruction of the electron tomographic data of stained plastic sections of fixed cells.

Acknowledgments

We would like to acknowledge Kèvin Knoops for sectioning, Erik Bos for cryo-sectioning and Bram de Visser for manufacturing of clip rings. RIK is financed by Netherlands SmartMix grant and the NIMIC partner organizations (www.real-nano.com) through NIMIC, a public-private program.

Appendix A. Supplementary information

Supplementary data associated with this article can be found in the online version at http://dx.doi.org/10.1016/j.ultramic.2013.06.015.

References

[1] M. Barcena, A.J. Koster, Electron tomography in life science, Seminars in Cell & Developmental Biology 20 (2009) 920–930.
[2] V. Lucic, F. Forster, W. Baumeister, Structural studies by electron tomography: from cells to molecules, Annual Review of Biochemistry 74 (2005) 833–865.

[3] F. Amat, D. Castano-Diez, A. Lawrence, F. Moussavi, H. Winkler, M. Horowitz, Alignment of cryo-electron tomography datasets, Methods in Enzymology 482 (2010) 343–367.
[4] M. Gruska, O. Medalia, W. Baumeister, A. Leis, Electron tomography of vitreous sections from cultured mammalian cells, Journal of Structural Biology 161 (2008) 384–392.
[5] M.B. Braunfeld, A.J. Koster, J.W. Sedat, D.A. Agard, Cryo automated electron tomography: towards high-resolution reconstructions of plastic-embedded structures, Journal of Microscopy 174 (1994) 75–84.
[6] D.N. Mastronarde, Fiducial marker and hybrid alignment methods for single- and double-axis tomography, in: J. Frank (Ed.), Electron Tomography, Springer, New York, 2007, pp. 163–185.
[7] P.P. Pompa, L. Martiradonna, A.D. Torre, F.D. Sala, L. Manna, V.M. De, F. Calabi, R. Cingolani, R. Rinaldi, Metal-enhanced fluorescence of colloidal nanocrystals with nanoscale control, Nature Nanotechnology 1 (2006) 126–130.
[8] N. Clement, G. Patriarche, K. Smaali, F. Vaurette, K. Nishiguchi, D. Troadec, A. Fujiwara, D. Vuillaume, Large array of sub-10-nm single-grain Au nanodots for use in nanotechnology, Small 7 (2011) 2607–2613.
[9] A. Pimpkin, W. Srituravanich, Reviews on micro- and nanolithography techniques and their applications, Engineering Journal 16 (2011) 37–55.
[10] H. Seidel, L. Csepregi, A. Heuberger, H. Baumgartel, Anisotropic etching of crystalline Silicon in alkaline solutions, Journal of the Electrochemical Society 137 (1990) 3612–3632.
[11] K.R. Williams, K. Gupta, M. Wasilik, Etch rates for micromachining processes – part II, Journal of Microelectromechanical Systems 12 (2003) 761–778.
[12] K. Knoops, M. Kikkert, S.H. Worm, J.C. Zevenhoven-Dobbe, Y. van der Meer, A. J. Koster, A.M. Mommaas, E.J. Snijder, SARS-coronavirus replication is supported by a reticulovesicular network of modified endoplasmic reticulum, PLoS Biology 6 (2008) e226.
[13] J.R. Kremer, D.N. Mastronarde, J.R. McIntosh, Computer visualization of three-dimensional image data using IMOD, Journal of Structural Biology 116 (1996) 71–76.
[14] J. Pierson, J.J. Fernandez, E. Bos, S. Amini, H. Gnaegi, M. Vos, B. Bel, F. Adolfsen, J.L. Carrascosa, P.J. Peters, Improving the technique of vitreous cryo-sectioning for cryo-electron tomography: electrostatic charging for section attachment and implementation of an anti-contamination glove box, Journal of Structural Biology 169 (2010) 219–225.
[15] D. Rhinow, W. Kuhlbrandt, Electron cryo-microscopy of biological specimens on conductive titanium-silicon metal glass films, Ultramicroscopy 108 (2008) 698–705.
[16] F. Amat, F. Moussavi, L.R. Comolli, G. Elidan, K.H. Downing, M. Horowitz, Markov random field based automatic image alignment for electron tomography, Journal of Structural Biology 161 (2008) 260–275.
[17] S.B. van, M.J. van Bruggen, P. Kruit, Design approach for a multi-beam electron beam-induced deposition system, Scanning 27 (2005) 158–159.